frontiers in Physics

ORIGINAL RESEARCH
published: 20 October 2021
doi: 10.3389/fphy.2021.749501

Properties and Sensing Performance of THz Metasurface Based on Carbon Nanotube and Microfluidic Channel

Yue Wang[1]*, *Xiaoju Zhang*[1,2], *Tao Zhou*[1], *Yongqiang Zhu*[1], *Zijian Cui*[1] and *Kuang Zhang*[3]

[1]Key Laboratory of Ultrafast Photoelectric Technology and Terahertz Science in Shaanxi, Xi'an University of Technology, Xi'an, China, [2]Engineering University of PAP Xi'an, Xi'an, China, [3]Department of Microwave Engineering, School of Electronics and Information Engineering, Harbin Institute of Technology Harbin, Harbin, China

Carbon-based metamaterials are expected to lead to biological and chemical sensing because of their fast electron transfer rate, good biocompatibility, and high absorption ratios. In this work, we integrate carbon nanotubes metasurface (CM) and microfluidic channel (MC) for a composite terahertz (THz) metasurface (CMMC). The absorption properties and sensing performance of the proposed composite metasurface have been studied. It is observed that the absorption is nearly 71.8% at 0.96 THz and 92.4% at 1.65 THz, respectively. The variation of response with refractive index of the analytes for the proposed CMMC is investigated and it is found that the frequency and intensity of the resonance absorption peak at 0.96 THz f_1 decrease obviously with the increase of the refractive index of the analytes. Owing to the coupling of the CM and MC in the microfluidic channel, the interaction between the incident THz wave and analytes has been enhanced, and the frequency and intensity sensitivities has achieved 254 GHz/RIU and 314/RIU, respectively. In addition, the influence of the structural parameters of the proposed CMMC on the absorption characteristics is also studied in detail. The results shown that the absorption properties of the CMMC can be adjusted by changing the structural parameters, which will provide a guideline for design. The proposed CMMC will facilitate the realization of carbon nanotube metamaterials sensing applications, and, when combined with microfluidic channel, will lead to large-area THz biological and chemical sensing.

Keywords: carbon nanotubes, THz, metasurface, microfluidic channel, refractive index sensing

OPEN ACCESS

Edited by:
Yingxin Wang,
Tsinghua University, China

Reviewed by:
Bo Zhang,
Capital Normal University, China
Lin Chen,
University of Shanghai for Science and Technology, China

****Correspondence:***
Yue Wang
wangyue2017@xaut.edu.cn

Specialty section:
This article was submitted to Optics and Photonics, a section of the journal Frontiers in Physics

Received: *29 July 2021*
Accepted: *30 September 2021*
Published: *20 October 2021*

Citation:
Wang Y, Zhang X, Zhou T, Zhu Y, Cui Z and Zhang K (2021) Properties and Sensing Performance of THz Metasurface Based on Carbon Nanotube and Microfluidic Channel. Front. Phys. 9:749501. doi: 10.3389/fphy.2021.749501

INTRODUCTION

Artificial electromagnetic metasurfaces composed of various periodically arranged subwavelength structures have recently generated great interest [1–3]. Owing to the distinguished electromagnetic response which cannot be realized by in nature materials, artificial metasurfaces offer essential information for various applications in imaging, sensing, and other fields [4–8]. With the development of terahertz (THz) spectroscopy and the micro-nanofabrication technology [9], THz spectroscopy technology based on metamaterials has become a potential detection method. On one hand, the resonances of the artificial electromagnetic metasurfaces whose electromagnetic response can be controlled by design [10] are more sensitive to the change of the dielectric environment [11]. On the other hand, THz spectroscopy technology has some unique advantages such as label-free, non-invasive, and non-destructive characteristics

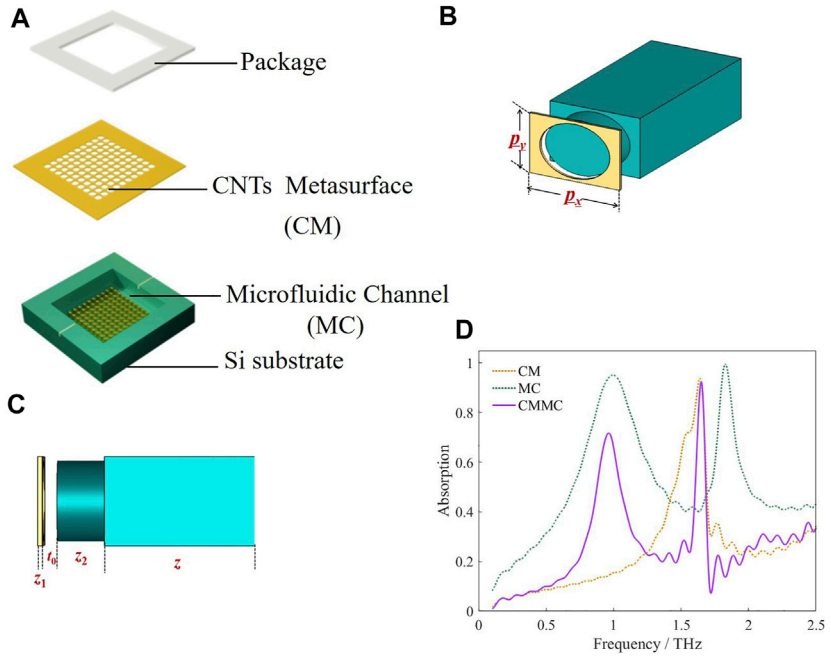

FIGURE 1 | (A) Illustration of the CMMC. **(B)** The unit cell geometry of the CMMC. **(C)** The side view of the unit cell of the CMMC. **(D)** The absorption spectra of the CMMC and other two structures only with CM or MC.

[12]. Therefore, THz metasurface have been utilized for chemical, biological and other sensing applications [13–19].

At present, considerable research efforts have been devoted to metallic metasurface based on metal structural unit cell, but the extended application of the traditional metallic metasurface is limited by the inherent losses, inflexibility, and high processing cost [20, 21]. As a kind of carbon-based material [22, 23], carbon nanotubes (CNTs) film has some merits, such as fast electron transfer rate, good biocompatibility, low-cost, and freely bendable flexibility [24–27]. The metamaterials based on CNTs film are also sensitive to changes in the dielectric environment because of the resonances. All these merits indicate that CNTs-based metamaterials are suitable for THz sensing applications. In addition, the spatial overlap between the analytes and the electric field can enhance the interaction between the analytes and the incident THz wave, which means that it is particularly important to locate the analytes where the concentration of electric field is the largest. Therefore, microfluidic channel maybe provide a new strategy for THz sensing applications [28, 29].

In this paper, we integrate the CNTs metasurface (CM) with periodic elliptical pore structure and the silicon microfluidic channel (MC) with periodic elliptic cylindrical structure at the bottom to form a composite THz metasurface (CMMC). The light-matter interaction between the THz wave and the analytes can be improved by the integration of CM and MC. The absorption spectrum of the designed CMMC is studied, and other two structures only with CM or MC are also investigated for comparison. The CMMC can achieve narrowband absorption, the absorption is nearly 71.8% at 0.96 THz and 92.4% at 1.65 THz, respectively. Because the resonance of the CMMC is sensitive to the changes of the dielectric environment, the refractive index (RI) sensing capabilities of the proposed CMMC are investigated in detail. The study reveals that the resonance peaks shift depends on the change of the refractive index of the analytes. Further calculation results show that the frequency and intensity of f_1 decrease obviously with the increase of refractive index of the analytes. The influence of structural parameters of the CMMC on the absorption properties is also studied and the results can be used as a guideline for design. The proposed CMMC combining the advantages of CM and MC, provides another sensing strategy with tunable resonance characteristics, can be applied for biological and chemical detection [14, 30].

STRUCTURE AND DESIGN

As shown in **Figure 1A**, the proposed CMMC is integrated by CNTs metasurface and microfluidic channel. The CNTs film used in the simulation is treated as composite material, the conductivity is extracted from experimental spectra, which has been reported in our previous work [31]. The microfluidic channel is made of high doped N-type silicon (Si) substrate with doping concentration $b = 2.91 \times 10^{18}\,\mathrm{cm}^{-3}$. A square sample pool with a periodic elliptic cylindrical structure at the bottom was etched on the high doped N-type silicon substrate. The permittivity of the highly doped silicon was descripted by using the Drude dispersion model [32]. It should be noted that the bottom of the sample pool is not smooth and flat, but a metasurface with periodic structure. The high doped N-type

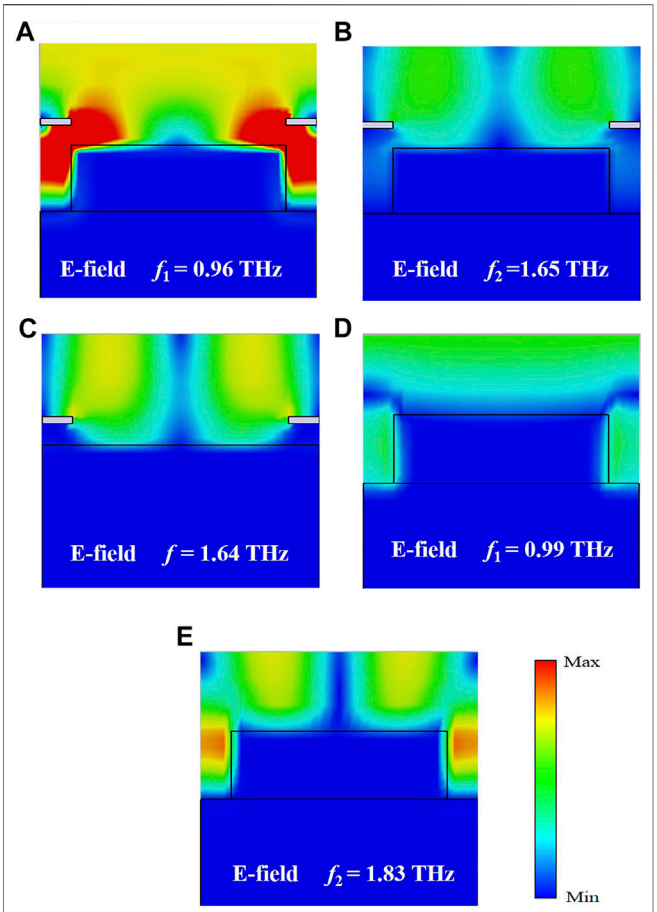

FIGURE 2 | (A,B) Electric field intensity distribution of the proposed CMMC at 0.96 THz and 1.65 THz; **(C)** Electric field intensity distribution of the CM at 1.64 THz. **(D,E)** Electric field distribution of the MC at 0.99 THz and 1.83 THz.

silicon metasurface which can be prepared by lithography shows advantage for simple fabrication. In our design, the square sample pool with a periodic elliptic cylindrical structure at the bottom not only supports the CM as substrate, but also improves the performance of the CMMC. The CNTs film etched periodic elliptical pore is coated on the top of the square sample pool. After that, a microfluidic channel is formed by integrating the CNTs film metasurface and microfluidic channel. Finally, a packaging layer etched with 6 × 6 mm detection window is pressed on the surface of the CM. The unit cell of the CMMC illustrated in **Figures 1B,C**, it is composed of CM and MC. The values of the geometric parameters are set as follows: the repeat period is p_x = 180 μm, and p_y = 110 μm; the thickness of CNTs film is z_1 = 5 μm; the radius of the major and minor axis of the elliptical pore in the CNTs film are R_{x1} = 70 μm and R_{y1} = 50 μm, respectively; the height of the elliptic cylinder is z_2 = 50 μm; the radius of the major and minor axis of the ellipse elliptic cylinder are R_x = 70 μm and R_y = 50 μm, respectively; the thickness of the silicon substrate is z = 350 μm; the etching depth of the sample pool is t_0 = 15 μm. Here, the height of the microfluidic channel is determined by the etching depth of the sample pool.

RESULTS AND DISCUSSION

Absorption Characteristics With Different Structures

Figure 1D shows the simulation absorption spectra of the designed CMMC and other two structures only with CM or MC. As shown in **Figure 1D**, the CMMC exhibits two obvious resonant absorption peaks, f_1 is located at 0.96 THz with absorption of 71.8%, and the resonant peak appears at 1.65 THz f_2 with absorption of 92.4%.

In order to reveal the physical mechanism of the resonance, the electric field distribution of the proposed CMMC, and other two structures only with CM or MC are investigated. **Figures 2A,B** show the electric field distribution of CMMC at the resonant frequency of 0.96 and 1.65 THz. As shown in **Figure 2A**, most of the field intensity is concentrated in the microfluidic channel formed by the integration of CM on the top and MC at the bottom, which will be filled with analytes during sensing detection. It is obvious that the microfluidic channel increases the overlap of space and improves the light-matter interaction between the analytes and the incident THz wave.

From **Figure 2B,** the intensity of the electric field at 1.65 THz is focused on the surface of the CMMC and the resonance is a surface mode. The electric field intensity distribution of the CM at 1.64 THz is shown in **Figure 2C**, the field intensity is mostly located on the surface, which is also surface mode. According to **Figure 2D,E,** the electric field intensity distributions of MC at 0.99 and 1.83 THz are confined on the surface and the gap between adjacent elliptic cylinders along x direction. Although the electric field at 1.83 THz is also concentrated on the surface and the gap between adjacent elliptical cylinders, which is similar to that of 0.99 THz, but the electric field on the surface is not uniformly distributed, which is a surface mode. By comparing the electric field distribution of the three different structures, it is found that the resonant absorption peak at 0.96 THz is related to the coupling of the modes, which increases the interaction between the incident THz wave and the analytes in the microfluidic channel.

Refractive Index Sensing Characteristics of the Proposed THz Metasurface

To study the sensing characteristics of the CMMC, we investigate the absorption spectra of CMMC with different refractive index of analytes n. The height of the microfluidic channel is fixed as 15 μm and the filling thickness of the analytes is t = 45 μm. The range of refractive index from 1.0 to 2.0 covers most bio and chemo specimens, such as DNA, RNA, and amino acids proteins [33, 34].

As shown in **Figure 3A**, it is obvious that the resonant absorption peak at 0.96 THz (f_1) is more sensitive to the change of refractive index than that at 1.64 THz (f_2). In order to gain a further understanding of the different sensitivity of the two peaks to the change of refractive index, we investigate the resonance mechanism in-depth. As shown in **Figure 2A,B,** most of the field intensity is concentrated in the microfluidic channel which will be filled with analytes with different refractive index

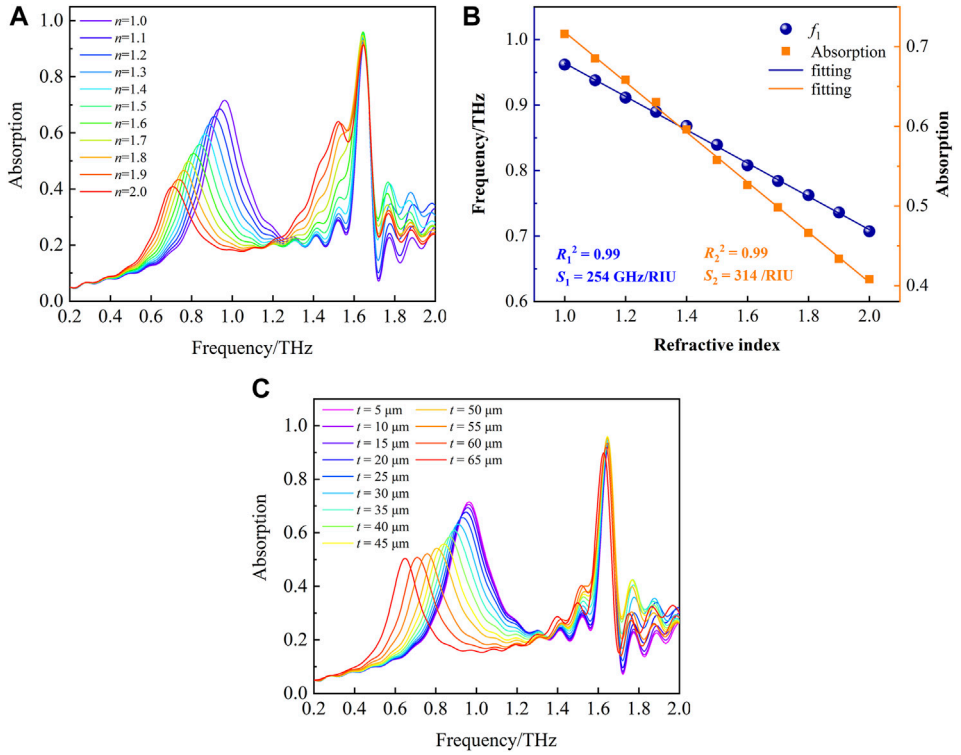

FIGURE 3 | (A) Absorption spectra for the analytes with different refractive indices. **(B)** Regression curves fitted for the refractive indices increases from 1.0 to 2.0, where the filling thickness of the analytes t = 45 μm. **(C)** Absorption spectra of the proposed composite metasurface with different filling thickness, where the refractive index of the analytes is n = 1.5.

during sensing detection and the concentrated electric field resulting from the mode coupling of the CM and MC will improve the light-matter interaction between the analytes and the THz wave. In contrast, the electric field at 1.65 THz is concentrated on the surface, the resonance is an obvious surface mode. Therefore, the resonance peak is not sensitive to changes of the refractive index of the analyte which is located in the microfluidic channel. As shown in **Figure 3A**, the resonant absorption frequency decreases when the refractive index of the analytes in the microfluidic channel increase. Obvious red shift of f_1 is observed, and the total shift is 254 GHz, which indicates that any change in the liquid permittivity will cause the parallel shift of resonance frequency.

In our case, considering the height of the microfluidic channel (t = 15 μm) is far less than the repeat period (p_x = 180 μm, p_y = 110 μm), the gap plasmon model can be used for explaining the physical mechanism [35–37]. In such a model, the resonance at 0.96 THz is caused by the Fabry-Perot resonances in the CNTs/analytes/Si cavity [36].

$$\frac{2\pi\omega n}{\lambda} + \varphi = k\pi \tag{1}$$

where w is the coverage width of the CM ($w = p_x - 2R_{x1}$), n is the effective index of the gap plasmon, λ is the resonance wavelength, φ is reflection phase, and k is the order of resonance. In addition, according to the distribution of electric field in **Figures 2A,D**, the resonance at 0.96 THz is caused not only by the Fabry-Perot resonances in the CNTs/analytes/Si cavity, but also by the Si elliptic cylinder.

It is observed clearly that the resonant frequency decreases as the refractive index of the analytes in the microfluidic channel increases, and f_1 is more sensitive to the change of the refractive index. As shown in **Figure 3B**, the frequency decreases linearly with refractive index increasing, there is a good linear relationships between the position of f_1 and the refractive indices of analytes with the regression coefficients of 0.99 (the blue fitting line). The frequency sensitivity S_1 of the proposed CMMC integrated CNTs film metasurface and the microfluidic channel is defined by frequency shift per refractive index unit, which can be calculated as:

$$S_1 = \frac{\Delta f}{\Delta n} \tag{2}$$

where, S_1 is frequency sensitivity, whose unit is GHz/RIU (RIU = Refractive Index Unit), Δn is the change of the refractive index; Δf is the change of resonant frequency with different n. According to **Eq. 2** and **Figure 3B**, the frequency sensitivity S_1 of the CMMC which equaled to the slope of the blue line in **Figure 3B**, reached 254 GHz/RIU.

In addition, as the refractive index of the analytes increase, the amplitude of f_1 also decreases. The intensity of the resonance decreases linearly with refractive index

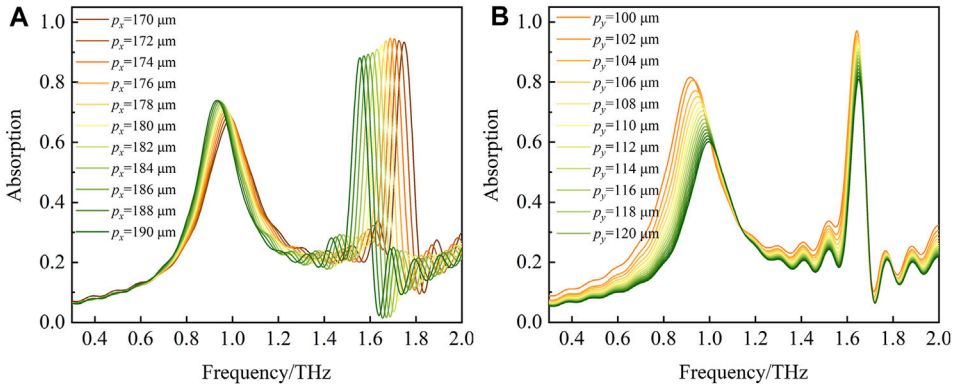

FIGURE 4 | (A) The absorption spectra of the CMMC with p_x increasing from 170 to 190 μm, where the p_y is fixed at 110 μm. **(B)** The absorption spectra of the CMMC with p_y increasing from 100 to 120 μm, where the p_x is fixed at 180 μm.

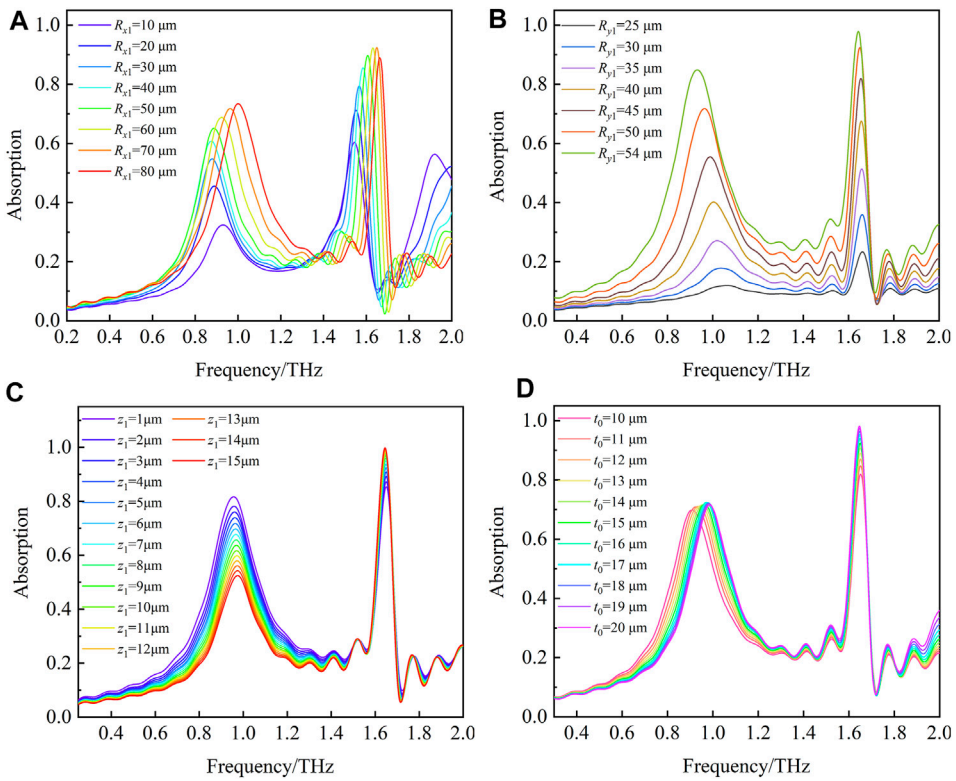

FIGURE 5 | (A) The absorption spectra with the major axis radius of the elliptical pore in the CNTs film R_{x1} increasing from 10 to 70 μm, where R_{y1} is fixed as 50 μm. **(B)** The absorption spectra with the minor axis radius of the elliptical pore in the CNTs film R_{y1} increasing from 25 to 54 μm, where R_{x1} is fixed as 70 μm. **(C)** The absorption spectra with different thickness of the CNTs film z_1. **(D)** The absorption spectra of the CMMC with the height of the microfluidic channel increasing from 10 to 20 μm.

increasing, a good linear relationship between the intensity of resonant peak and the refractive indiex of analytes with the regression coefficients of 0.99 is observed from orange fitting line of **Figure 3B**. Therefore, apart from the sensitivity defined by the frequency shift, the variation of intensity ΔI can also be used for refractive index sensing. The intensity sensitivity S_2 of the proposed CMMC is defined dip the variation of intensity ΔI per refractive index unit, which could be characterized as:

$$S_2 = \frac{\Delta I}{\Delta n} \tag{3}$$

where, the unit of S_2 is/RIU, ΔI is the variation of the intensity of resonance absorption peak with different n. The intensity

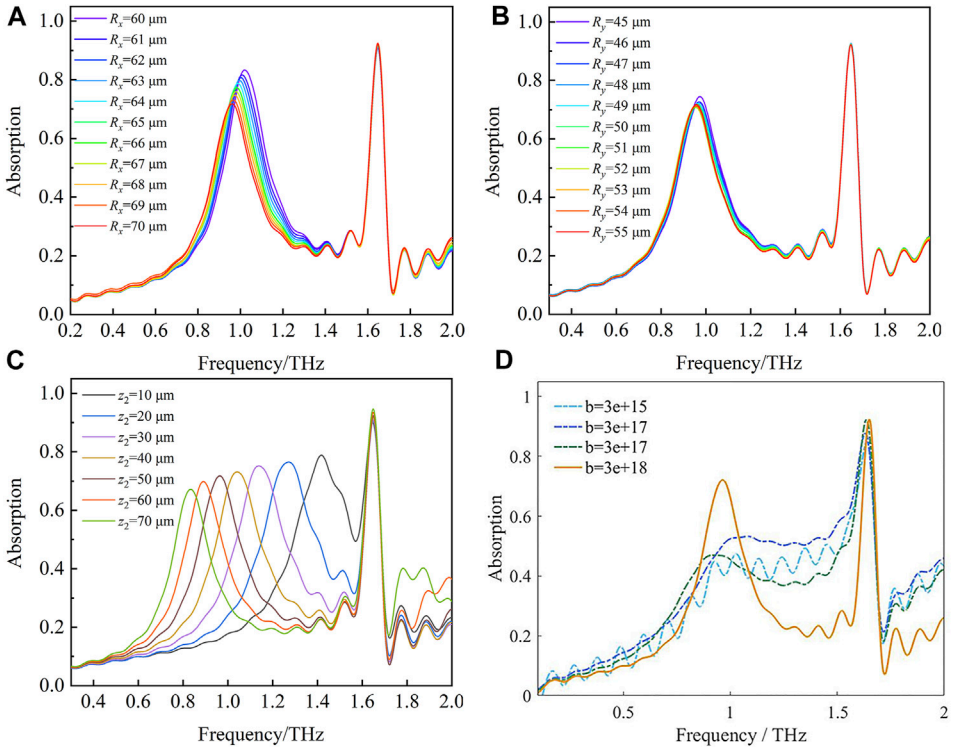

FIGURE 6 | (A) The absorption spectra with the major axis radius of the Si elliptic cylinder R_x increasing from 60 to 70 μm, where R_y is fixed as 50 μm. **(B)** The absorption spectra with the minor axis radius of the Si elliptic cylinder R_y increasing from 45 to 55 μm, where R_x is fixed as 70 μm. **(C)** The absorption spectra with different height of the elliptic cylinder z_2. **(D)** The absorption spectra with different doping concentration of silicon.

sensitivity S_2 of CMMC, (i.e. the slope of the orange fitting lines in **Figure 3B**), reached 314/RIU. That means that both the variation of frequency shift Δf and intensity ΔI can be used for refractive index sensing. **Figure 3C** shows the influence of thickness of the analytes on the absorption spectrum, assuming the RI of the analytes is 1.5. As the thickness of the analytes t increases from 5 to 65 μm, both the frequency and intensity of f_1 decrease, which indicates that the CMMC is also sensitive to the thickness of the analytes. Due to the increase of the filling thickness, the analytes is gradually closer to the region with the largest field intensity, and the interaction between the THz wave and analytes is further enhanced, leading to a more obvious frequency shift, which indicates that the filling thickness of the analytes has an effect on the sensing performance of the CMMC.

The Influence of the Structural Parameters on Absorption Characteristics of the THz Metasurface

In order to guide the structural design of the CMMC, the absorption characteristics with different structural parameters are investigated. **Figure 4A** shows the influence of the period in the x-direction p_x on the absorption. As p_x increases, f_2 shows an obvious red shift, while f_1 has a relatively weak red shift. On the contrary, as shown in **Figure 4B**, with the period in the y-direction p_y increasing, the resonance frequency of f_1 blue shifts while the amplitude gradually decreases. However, the resonance frequency of f_2 is almost unchanged, but the amplitude is significantly reduced. It is obvious that the variations of the period in x-direction or the y-direction have different effects on the two resonance peaks, implying that the resonance mechanisms of the two peaks are different, which is consistent with the analysis of the electric field distribution in **Figures 2A,B**.

Due to the importance of CM in the proposed CMMC, we studied the effect of the structural parameters of CM on the absorption characteristics. As shown in **Figure 5A**, as the major axis radius of the elliptical pore on the CNTs film R_{x1} increases from 10 to 80 μm, the amplitude of f_1 gradually increases, which is resulted from the enlarged aperture and enhanced resonance. With R_{x1} increasing from 10 to 40 μm, the resonance frequency of f_1 decreases. However, the resonance frequency of f_1 increases when R_{x1} increases from 50 to 80 μm. The difference of the shift law might be contribute to the fact that the minor axis radius of the elliptical pore R_{y1} is fixed as 50 μm in this case, when R_{x1} is less than 50 μm (i.e. $R_{x1} < R_{y1}$), it means that the major axis of the elliptical pore is along the y direction; when R_{x1} is greater than 50 μm (i.e. $R_{x1} > R_{y1}$), the major axis is along the x direction. Therefore, the asymmetry of the elliptical structure in the x and y directions results in the difference of shift law of the resonance frequency. **Figure 5B** shows the effect of the change of R_{y1} on the absorption when R_{x1} is fixed at 70 μm ($R_{x1} > R_{y1}$). With the

increase of R_{y1}, f_1 has a slight red shift and the absorption intensity increases significantly. Owing to $R_{x1} > R_{y1}$, the major axis of the ellipse is in the x direction, and there is no critical point in the variation law of frequency. In this case, the increase of R_y1 has a significant effect on the absorption intensity, indicating that the absorption intensity strongly depends on R_y1.

The absorption spectra with different thickness of the CNTs film is shown in **Figure 5C**. As z_1 increases, the intensity of f_1 decreases linearly, but the position of the resonance peak is almost unchanged, which means that the shape and size of the periodic elliptical pore of the CNTs film metasurface affect the position of the peak, and the thickness of the CNTs film only affects the absorption intensity.

The height of the microfluidic channel of the CMMC t_0 is an important parameter for sensing application, the influence of the height of the microfluidic channel on the absorption spectrum is investigated. As shown in **Figure 5D**, as t_0 increasing from 10 to 20 μm, f_1 has a slight blue shift, but the amplitude is almost unchanged. Therefore, the integrated CMMC with different height of microfluidic channel can be designed for refractive index sensing according to practical application.

We also investigate the influence of the structural parameters of the microfluidic channel on the absorption. As shown in **Figure 6A**, with the major axis radius of the Si elliptic cylinder R_x increasing from 60 to 70 μm, both the amplitude and the resonance frequency of f_1 decrease. However, according to **Figure 6B**, compared with R_x, as the minor axis radius of the Si elliptic cylinder R_y increases from 45 to 55 μm, the changes of the amplitude and the frequency of f_1 are not obvious, which results from the electric field distribution of f_1. As shown in **Figure 2A**, most of the electric field of f_1 is along x direction and the intensity is concentrated in the microfluidic channel formed by CM on the top and MC at the bottom. As a result, the amplitude and the frequency of f_1 are not strongly dependent on R_y. **Figure 6C** shows the absorption spectra with different height of the elliptic cylinder z_2. In particular, as z_2 increases from 10 to 70 μm, the resonance frequency of f_1 decreases significantly, the resonant peak has a significant red shift, which imply that the position of f_1 can be controlled by the height of the elliptic cylinder, which provides an idea for sensing and detection in a wider range. Doping concentration is an important parameter affecting the dielectric properties of silicon. Therefore, we investigated the influence of doping concentration on the absorption properties of the proposed CMMC. In **Figure 6D**, as the doping concentration increases, the resonance absorption is significantly enhanced. As discussed above, it is worth noting that the change of structural parameters of silicon microfluidic channel has little effect on f_2, which further indicates that f_2 is a surface mode mainly determined by CM. The results is agree with the electric field distribution in **Figures 2B,C**.

CONCLUSION

To summarize, we proposed a composite THz metasurface CMMC for sensing, which integrates the CNTs metasurface with periodic elliptical pore structure and the microfluidic channel with periodic elliptic cylindrical structure at the bottom. The properties and sensing performance of the CMMC have been investigated. The study reveals that both the resonant frequency and the intensity of f_1 have a linear response with increase in refractive index of the analytes in the microfluidic channel and the sensitivities can achieve 254 GHz/RIU and 314/RIU, respectively, which is attributed to coupling of the CM and MC and the enhanced interaction between the THz wave and the analytes. The influence of the structural parameters on the absorption characteristics illustrates that the absorption performance of the proposed CMMC can be adjusted by changing the structural parameters, which will provide a guideline for the CMMC design. The demonstrated CMMC will facilitate the realization of carbon nanotube metamaterials sensing applications, and, when combined with microfluidic channel, will provide another sensing strategy with tunable resonance characteristics, and lead to large-area THz biological and chemical sensing.

DATA AVAILABILITY STATEMENT

The raw data supporting the conclusion of this article will be made available by the authors, without undue reservation.

AUTHOR CONTRIBUTIONS

YW conceived the idea and led the design; KZ modified the frame. ZC finished the Figure preparation, TZ and YZ collected the references. YW and XZ finished the whole manuscript writing and the manuscript modification, TZ and XZ contributed to the proofreading, and all authors listed approved it for publication.

FUNDING

This work was supported in part by the National Natural Science Foundational of China under Grant 61975163, and in part by the Natural Science Foundation of Shaanxi Province under Grant 2020JZ-48, and in part by the Youth Innovation Team of Shaanxi Universities under Grant 21JP084, and in part by Open Project of Key Laboratory of Engineering Dielectrics and Its Applications, Ministry of Education under Grant KEY1805.

REFERENCES

1. Glybovski S. B., Tretyakov S. A., Belov P. A., Kivshar Y. S., and Simovski C. R.. Metasurfaces: From Microwaves to Visible. *Phys Rep* (2016) 634:1–72. doi:10.1016/j.physrep.04.004
2. Cojocari M. V., Schegoleva K. I., and Basharin A. A.. Blueshift and Phase Tunability in Planar THz Metamaterials: the Role of Losses and Toroidal Dipole Contribution. *Opt Lett* (2017) 42:1700–3. doi:10.1364/ol.42.001700
3. Wang S., Zhao X., Wang S., Li Q., Zhu J., and Han L.. The Investigation of the Electromagnetic Coupling Effect in Terahertz Toroidal Metasurfaces and

Metamaterials. *J Mater Res Tech* (2020) 9:3935–42. doi:10.1016/j.jmrt.2020.02.019
4. Padilla W. J., Taylor A. J., Highstrete C., Lee M., and Averitt R. D.. Dynamical Electric and Magnetic Metamaterial Response at Terahertz Frequencies. *Phys Rev Lett* (2006) 96:107401. doi:10.1103/PhysRevLett.96.107401
5. Qian Q., Fan L., Zhao L., and Wang C.. Non-metallic and Angular-Insensitive Metasurface Transmissive Long-Pass Filter in the Visible and Near-Infrared Regions. *Opt Lett* (2020) 45:359–62. doi:10.1364/OL.384358
6. Wang Z., Liu J., Ding X., Zhao W., Zhang K., Li H., et al. Three-Dimensional Microwave Holography Based on Broadband Huygens' Metasurface. *Phys Rev Appl* (2020) 13:7. doi:10.1103/PhysRevApplied.13.014033
7. Chen M., Wang Y. X., and Zhao Z. R.. Localized Electromagnetic Resonance Enabled THz Photo Thermo Electric Detection in Graphene. *Front Phys* (2020) 8:8. doi:10.3389/fphy.2020.00216
8. Liu W., Yang Q., Xu Q., Jiang X., Wu T., Wang K., et al. Multifunctional All-Dielectric Metasurfaces for Terahertz Multiplexing. *Adv Opt Mater.* (2021) 9:2100506. doi:10.1002/adom.202100506
9. Zhang Z., Zhu Z., Yuan M., Minghui Li M. H., You G., Chen L., et al. Predict Sample's Line Positions of Absorption Peaks in Terahertz Band with the Forced Radiation Intensity of Molecular Electric Dipoles. *Opt Commun* (2020) 458:124848. doi:10.1016/j.optcom.2019.124848
10. Beruete M., and Jáuregui-López I.. Terahertz Sensing Based on Metasurfaces. *Adv Opt Mater.* (2020) 8:1900721. doi:10.1002/adom.201900721
11. Zhang K., Yuan Y., Ding X., Ratni B., Burokur S. N., and Wu Q.. High-Efficiency Metalenses with Switchable Functionalities in Microwave Region. *ACS Appl Mater Inter* (2019) 11:28423–30. doi:10.1021/acsami.9b07102
12. Lu Y., Wang X.-K., Sun W.-F., Feng S.-F., Ye J.-S., Han P., et al. Reflective Single-Pixel Terahertz Imaging Based on Compressed Sensing. *IEEE Trans Thz Sci Technol* (2020) 10:495–501. doi:10.1109/TTHZ.2020.2982350
13. Wang Y., Cui Z., Zhang X., Zhang X., Zhu Y., Chen S., et al. Excitation of Surface Plasmon Resonance on Multiwalled Carbon Nanotube Metasurfaces for Pesticide Sensors. *ACS Appl Mater Inter* (2020) 12:52082–8. doi:10.1021/acsami.0c10943
14. Geng Z., Zhang X., Fan Z., Lv X., and Chen H.. A Route to Terahertz Metamaterial Biosensor Integrated with Microfluidics for Liver Cancer Biomarker Testing in Early Stage. *Sci Rep* (2017) 7:11. doi:10.1038/s41598-017-16762-y
15. Wang Y., Zhu D., Cui Z., Yue L., Zhang X., Hou L., et al. Properties and Sensing Performance of All-Dielectric Metasurface THz Absorbers. *IEEE Trans Thz Sci Technol* (2020) 10:599–605. doi:10.1109/tthz.2020.3010164
16. Lin S., Xu X., Hu F., Chen Z., Wang Y., Zhang L., et al. Using Antibody Modified Terahertz Metamaterial Biosensor to Detect Concentration of Carcinoembryonic Antigen. *IEEE J Select Top Quan Electron.* (2021) 27:1–7. doi:10.1109/jstqe.2020.3038308
17. Yang X., Zhao X., Yang K., Liu Y., Liu Y., Fu W., et al. Biomedical Applications of Terahertz Spectroscopy and Imaging. *Trends Biotechnol* (2016) 34:810–24. doi:10.1016/j.tibtech.2016.04.008
18. Xu W., Xie L., and Ying Y.. Mechanisms and Applications of Terahertz Metamaterial Sensing: a Review. *Nanoscale* (2017) 9:13864–78. doi:10.1039/C7NR03824K
19. Wang Y. X., Wu W. D., and Zhao Z. R.. Recent Progress and Remaining Challenges of 2D Material-Based Terahertz Detectors. *Infrared Phys Technol* (2019) 102:14. doi:10.1016/j.infrared.2019.103024
20. Kabashin A. V., Evans P., Pastkovsky S., Hendren W., Wurtz G. A., Atkinson R., et al. Plasmonic Nanorod Metamaterials for Biosensing. *Nat Mater* (2009) 8:867–71. doi:10.1038/nmat2546
21. Boltasseva A., and Atwater H. A.. Low-Loss Plasmonic Metamaterials. *Science* (2011) 331:290–1. doi:10.1126/science.1198258
22. Tepliakov N. V., Kundelev E. V., Khavlyuk P. D., Xiong Y., Leonov M. Y., Zhu W., et al. sp2-sp3-Hybridized Atomic Domains Determine Optical Features of Carbon Dots. *ACS Nano* (2019) 13:10737–44. doi:10.1021/acsnano.9b05444
23. Liu B., Zhu W., Gunapala S. D., Stockman M. I., and Premaratne M.. Open Resonator Electric Spaser. *Acs Nano* (2017) 11:12573–82. doi:10.1021/acsnano.7b06735
24. Liu K., Sun Y., Chen L., Feng C., Feng X., Jiang K., et al. Controlled Growth of Super-aligned Carbon Nanotube Arrays for Spinning Continuous Unidirectional Sheets with Tunable Physical Properties. *Nano Lett* (2008) 8:700–5. doi:10.1021/nl0723073
25. Nikolaenko A. E., De Angelis F., Boden S. A., Papasimakis N., Ashburn P., Di Fabrizio E., et al. Carbon Nanotubes in a Photonic Metamaterial. *Phys Rev Lett* (2010) 104:4. doi:10.1103/PhysRevLett.104.153902
26. Zhao J., Zhang W., Sherrell P. Razal J. M., Huang X.-F., Minett A. I., et al. Carbon Nanotube Nanoweb-Bioelectrode for Highly Selective Dopamine Sensing. *ACS Appl Mater Inter* (2012) 4:44–8. doi:10.1021/am201508d
27. Liu S. F., Petty A. R., Sazama G. T., and Swager T. M.. Single-Walled Carbon Nanotube/Metalloporphyrin Composites for the Chemiresistive Detection of Amines and Meat Spoilage. *Angew Chem Int Ed* (2015) 54:6554–7. doi:10.1002/anie.201501434
28. Xu J., Liao D., Gupta M., Zhu Y., Zhuang S., Singh R., et al. Terahertz Microfluidic Sensing with Dual-Torus Toroidal Metasurfaces. *Adv Opt Mater.* (2021) 9:2100024. doi:10.1002/adom.202100024
29. Chen L., Yin H, Chen L., and Zhu Y.. Ultra-sensitive Fluid Fill Height Sensing Based on Spoof Surface Plasmon Polaritons. *J Electromagn Waves Appl* (2017) 32:471–82. doi:10.1080/09205071.2017.1395367
30. Keshavarz A., and Vafapour Z. Sensing Avian Influenza Viruses Using Terahertz Metamaterial Reflector. *IEEE Sensors J* (2019) 19:5161–6. doi:10.1109/jsen.2019.2903731
31. Wang Y., Cui Z., Zhu D., Zhang X., and Qian L.. Tailoring Terahertz Surface Plasmon Wave through Free-Standing Multi-Walled Carbon Nanotubes Metasurface. *Opt Express* (2018) 26:15343–52. doi:10.1364/OE.26.015343
32. Enkrich C., Wegener M., Linden S., Burger S., Zschiedrich L., Schmidt F., et al. Magnetic Metamaterials at Telecommunication and Visible Frequencies. *Phys Rev Lett* (2005) 95:203901. doi:10.1103/physrevlett.95.203901
33. Zhang Y., Li T., Zeng B., Zhang H., Lv H., Huang X., et al. A Graphene Based Tunable Terahertz Sensor with Double Fano Resonances. *Nanoscale* (2015) 7:12682–8. doi:10.1039/c5nr03044g
34. Mcmeekin T. L., Groves M. L., and Hipp N. J.. *Refractive Indices of Amino Acids, Proteins, and Related Substances*. Washington, DC, USA: ACS Publications (1964) p. 54–66. doi:10.1021/ba-1964-0044.ch004
35. Nielsen M. G., Gramotnev D. K., Pors A., Albrektsen O., and Bozhevolnyi S. I.. Continuous Layer gap Plasmon Resonators. *Opt Express* (2011) 19:19310–22. doi:10.1364/OE.19.019310
36. Park J., Kang J.-H., Liu X., and Brongersma M. L.. Electrically Tunable Epsilon-Near-Zero (ENZ) Metafilm Absorbers. *Sci Rep* (2015) 5:9. doi:10.1038/srep15754
37. Li Z.-Y., Xu D.-X., Mckinnon W. R., Janz S., Schmid J. H., Cheben P., et al. Silicon Waveguide Modulator Based on Carrier Depletion in Periodically Interleaved PN Junctions. *Opt Express* (2009) 17:15947–58. doi:10.1364/OE.17.015947

Conflict of Interest: The authors declare that the research was conducted in the absence of any commercial or financial relationships that could be construed as a potential conflict of interest.

Publisher's Note: All claims expressed in this article are solely those of the authors and do not necessarily represent those of their affiliated organizations, or those of the publisher, the editors and the reviewers. Any product that may be evaluated in this article, or claim that may be made by its manufacturer, is not guaranteed or endorsed by the publisher.